

# Non-Hermitian State-to-State Analysis of Transport in Aggregates with Multiple Endpoints

Devansh Sharma and Amartya Bose\*



Cite This: *J. Chem. Theory Comput.* 2025, 21, 5858–5866



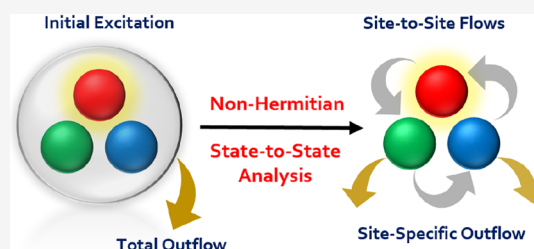
Read Online

ACCESS |

Metrics & More

Article Recommendations

**ABSTRACT:** Efficiency of quantum transport through aggregates with multiple endpoints or traps proves to be an emergent and a highly nonequilibrium phenomenon. We present an exact approach for computing the emergent time-scale and amount of extraction specific to particular traps, leveraging a non-Hermitian generalization of the recently introduced state-to-state transport analysis [Bose and Walters, *J. Chem. Theory Comput.* 2023, 19, 15, 4828–4836]. This method is able to simultaneously account for the coupling between various sites, the many-body effects brought in by the vibrations and environment held at a nonzero temperature, and the local extraction processes described by non-Hermitian terms in the Hamiltonian. In fact, our non-Hermitian state-to-state analysis goes beyond merely providing an emergent loss time-scale. It can parse the entire dynamics into the constituent internal transport pathways and loss to the environment. We demonstrate this method using examples of exciton transport in a lossy polaritonic cavity. The loss at the cavity and the extraction of the exciton from a terminal molecule provide competing mechanisms that our method helps to unravel, revealing nonintuitive physics. This non-Hermitian state-to-state analysis technique contributes an important link to understanding and elucidating the routes of transport in open quantum systems.



In fact, our non-Hermitian state-to-state analysis goes beyond merely providing an emergent loss time-scale. It can parse the entire dynamics into the constituent internal transport pathways and loss to the environment. We demonstrate this method using examples of exciton transport in a lossy polaritonic cavity. The loss at the cavity and the extraction of the exciton from a terminal molecule provide competing mechanisms that our method helps to unravel, revealing nonintuitive physics. This non-Hermitian state-to-state analysis technique contributes an important link to understanding and elucidating the routes of transport in open quantum systems.

## 1. INTRODUCTION

Various molecular aggregates function as wires, transferring charges and excitation from one end to the other. A prime example of such transport happening in nature is the so-called light-harvesting antenna complexes that absorb solar photons converting them into excitons, which are then shuttled to the reaction center where further reactions take place. The robustness and remarkable efficiency of the transport have made such photosynthetic systems a subject of extensive study.<sup>1–4</sup> Both from the perspective of fundamental understanding of these systems and the development of new materials, it is important to be able to quantify and simulate the efficiency of transport in these complex aggregates, which entails accurate simulation of dynamics. The large number of thermal degrees of freedom associated with the nuclear motion modulates the transport in a nonperturbative manner. Advanced wave function-based techniques like the density matrix renormalization group<sup>5–7</sup> or the multiconfiguration time-dependent Hartree,<sup>8,9</sup> while capable of handling non-perturbative system–environment interactions, still do not provide a practical route to simulation of these systems since they are unable to efficiently handle the large number of environmental modes that exist and the manifold of thermally accessible states.

Simulations involving a reduced density matrix provide a lucrative approach to understanding such nonequilibrium transport. Heijs et al.<sup>10</sup> and Cao and Silbey<sup>11</sup> have explored the relation between trapping time and efficiency, providing a

classical kinetic picture. Sener et al.<sup>12</sup> and others have explored the robustness of photosynthetic transport. Both approximate<sup>13,14</sup> and numerically exact methods<sup>15</sup> have been used to study the efficiency of quantum transport. Approximate methods are, however, often plagued by *ad hoc* assumptions that may fail for a particular system. In this context, numerically exact simulations using methods like hierarchical equations of motion<sup>16–20</sup> or the quasi-adiabatic propagator path integral<sup>21–27</sup> prove to be useful. They however require a full description of the endpoint from which the extraction happens, the sites to which the extraction happens, and their thermal environments to be able to determine the efficiency of the transport. Many transport aggregates may even have more than one endpoint or trap site. In such cases, this already challenging parametrization requirement is followed by an exponential growth of complexity due to a growth of the system Hilbert space with every extra trap site. Additionally, many processes like spontaneous emission from an excited state or loss from a leaky cavity in the case of a polaritonic system cannot be simply expressed as a well-characterized

**Received:** March 28, 2025

**Revised:** June 1, 2025

**Accepted:** June 4, 2025

**Published:** June 12, 2025



harmonic bath. These processes are naturally defined in terms of empirical time-scales. The grand challenge, therefore, is simulating the dynamics under empirical loss or extraction processes using numerically exact methods and then calculating the individual efficiencies of the different traps in a multitrap transport process.

The recently developed path integral Lindblad dynamics (PILD) framework<sup>28</sup> allows for a combination of Lindblad master equation to incorporate the loss or gain processes and numerically rigorous path integrals to account for the effects of the thermal environment. PILD has been used to study the effect of loss processes on exciton transport dynamics in the Fenna–Matthews–Olson complex<sup>28</sup> as well as on linear spectra of chiral aggregates.<sup>29</sup> In many cases, however, the use of non-Hermitian descriptions of the system coupled with path integrals to incorporate the dissipative environment provides an alternative route to study the dynamics.<sup>30</sup> While the nonunitarity of the propagators makes it inherently unsuited for spectra represented by correlation functions that couple the ground- and excited-state manifolds, non-Hermitian descriptions can be more than adequate for the study of lossy dynamics at a lower cost.

Understanding the time-scale of transport in aggregates with multiple monomers, while important, turns out to be quite challenging and nontrivial. Imagine an aggregate where, in the simplest case, the exciton or other quantum particle is extracted from one of the molecular sites, called the “trap” site, with a “local” time-scale of  $T$  time units. This  $T$  unit, which is the time-scale of extraction from an isolated site, is not the time-scale that one would actually observe in the aggregate. From the site of injection of the particle, it would have traveled to all accessible sites, and the fraction that is on the trap site would get extracted. This combination of nonequilibrium processes gives rise to an emergent time-scale  $\tau$  for the extraction as observed when a particular site is initially excited. It is this emergent time-scale,  $\tau$ , that is of interest to us. The problem becomes even more challenging when there are multiple trap sites with different local extraction time-scales,  $T_j$ , splitting the single exciton in different proportions. A relevant example of this multitrap transport turns out to be a single channel transport aggregate coupled to a lossy Fabry–Pérot cavity, with the loss at the cavity providing a different trapping channel, which, while useless to the transport, needs to be accounted for. The question then becomes one of assigning a site-specific emergent time-scale  $\tau_j$  and also understanding how much of the exciton is extracted ( $L_j^\infty$ ) from each such site.

In this work, we address this question of calculating the trap-specific transport efficiency corresponding to a multitrap transport aggregate in terms of the emergent site-specific time-scale,  $\tau_j$ , and the exciton extraction,  $L_j^\infty$ , by generalizing the recently derived state-to-state analysis<sup>31,32</sup> for Hamiltonians with non-Hermiticity, describing the rates of leakage from the different traps. This allows us to partition the total leakage of the system into the different sites, enabling us to build an intuitive picture for the efficiency of transport for a particular nonequilibrium initial condition without any ad hoc approximations. The non-Hermitian state-to-state transport method is developed in Section 2. Applications are demonstrated in Section 3 using a polaritonic trimer as an example, where an excitonic drain and the cavity loss provide the two competing trap mechanisms. (A different setup of the same polaritonic trimer is explored in Appendix A.) Finally, we end with some concluding remarks in Section 4.

## 2. METHOD

Consider the following Hamiltonian that describes an open quantum system:

$$\hat{H} = \hat{H}_0 + \hat{H}_{\text{env}} \quad (1)$$

where  $\hat{H}_0$  describes the system and  $\hat{H}_{\text{env}}$  describes the environment and its interaction with the system. For concreteness, let us assume that the system is described by a Frenkel Hamiltonian where each of the basis vectors  $|j\rangle$  represents the state where the quantum particle (charge or excitation) is on the  $j$ th site or molecule, and every other site is empty. The system, then, is generically described by the non-Hermitian operator

$$\hat{H}_0 = \sum_j \epsilon_j |j\rangle\langle j| + \sum_{j<k} h_{jk} (|j\rangle\langle k| + |k\rangle\langle j|) \quad (2)$$

where  $h_{jk} \in \mathbb{R}$  is the coupling or hopping parameter between the  $j$ th and the  $k$ th sites, and  $\epsilon_j \in \mathbb{C}$  is the energy of the system when the particle is on the  $j$ th site with the corresponding lifetime. The real part of  $\epsilon_j$  represents the site energy, while the imaginary part of  $\epsilon_j$ , wherever nonzero, represents the rate of loss or extraction from the  $j$ th site corresponding to the “local” decay time  $T_j$  with  $\text{Im}(\epsilon_j) = -\pi\hbar/T_j$ .

Some or all of the sites are individually coupled to thermal environments

$$\hat{H}_{\text{env}} = \sum_j \hat{H}_{\text{env}}^{(j)} \quad (3)$$

$$\hat{H}_{\text{env}}^{(j)} = \sum_b \frac{P_{jb}^2}{2} + \frac{1}{2} \omega_{jb}^2 x_{jb}^2 - c_{jb} x_{jb} \hat{S}_j \quad (4)$$

where the bath on the  $j$ th site is coupled to the system through the system operator  $\hat{S}_j$ . Each bath of harmonic oscillators is characterized by the oscillators’ frequencies  $\omega_{jb}$  and their corresponding couplings  $c_{jb}$ . These are related to the spectral density

$$J_j(\omega) = \frac{\pi}{2} \sum_b \frac{c_{jb}^2}{\omega_{jb}} \delta(\omega - \omega_{jb}) \quad (5)$$

which can be estimated using molecular dynamics simulations<sup>33,34</sup> or directly from experiments.

Consider an aggregate that is initially in the electronic ground state with the vibrations described by the thermal Boltzmann distribution corresponding to the ground electronic potential energy landscape. The aggregate ground states typically are uncorrelated and can be simply thought of as the direct product of the ground states of the constituent monomers. At  $t = 0$ , due to Franck–Condon (FC) excitation caused by a photon, one of the molecules, say the  $j$ th one, gets excited, leaving all others in the ground state and all of the nuclear distributions unchanged. This initial density matrix can be written as  $\rho(0) = \tilde{\rho}(0) \otimes e^{-\beta\hat{H}_{\text{env}}}/Z$ , where  $\tilde{\rho}(0) = |j\rangle\langle j|$ . The time-evolved reduced density matrix for such a separable initial condition can be written in terms of path integrals<sup>21,22</sup> (augmented for non-Hermitian systems<sup>30</sup>) as

$$\begin{aligned} \langle s_N^+ | \tilde{\rho}(N\Delta t) | s_N^- \rangle &= \sum_{s_j^\pm} \langle s_N^+ | \hat{U} | s_{N-1}^+ \rangle \langle s_{N-1}^+ | \hat{U} | s_{N-2}^+ \rangle \cdots \\ &\times \langle s_1^+ | \hat{U} | s_0^+ \rangle \langle s_0^+ | \tilde{\rho}(0) | s_0^- \rangle \langle s_0^- | \hat{U}^\dagger | s_1^- \rangle \\ &\times \cdots \langle s_{N-1}^- | \hat{U}^\dagger | s_N^- \rangle \times F[\{s_j^\pm\}] \end{aligned} \quad (6)$$

where  $\hat{U} = \exp(-i\hat{H}_0\Delta t/\hbar)$  is the forward propagator and  $\hat{U}^\dagger = \exp(i\hat{H}_0^\dagger\Delta t/\hbar)$  is the backward propagator. Notice that the non-Hermiticity of the system ( $\hat{H}_0 \neq \hat{H}_0^\dagger$ ) is taken into account in the definition of the backward propagator. In the path integral, the state of the system at the  $j$ th time point is  $s_j^\pm$ . The Feynman–Vernon influence functional,<sup>35</sup>  $F[\{s_j^\pm\}]$ , captures the system–environment interaction and makes the dynamics non-Markovian. It is dependent upon the spectral density.<sup>34</sup> In a condensed phase medium, the decay of the bath correlations with time allows for a truncation of the memory and iteration beyond this memory length. However, the cost of the simulation still increases exponentially with the memory length. Here, we use the time-evolving matrix product operator algorithm<sup>24</sup> adapted for non-Hermitian systems to do the simulations efficiently. This is implemented in the recently released `QuantumDynamics.jl` package.<sup>36</sup>

Now, because of the non-Hermiticity of  $\hat{H}_0$  and the consequent nonunitarity of the time-evolution,  $\text{Tr}[\tilde{\rho}(t)] \leq 1$ . In fact, the trace is a monotonically decreasing quantity, and for the single excitation subspace, the quantity  $L(t) = 1 - \text{Tr}[\tilde{\rho}(t)]$  is the amount of excitation that has leaked out of the system. As a simple example, consider excitation transport in an excitonic trimer of identical monomers, each with a constant nearest-neighbor electronic coupling  $h_{jk} = -h = -181.5 \text{ cm}^{-1} \delta_{k,j+1}$ . This is representative of typical electronic couplings in bacteriochlorophyll chains that have an absorption maximum around 800 nm.<sup>37–39</sup> For the purpose of dynamics, a datum-level shift in the excitation energies can be introduced. We set  $\text{Re}(\epsilon_j) = \epsilon = 0 \text{ cm}^{-1}$ . An exciton drain is also introduced on the third monomer with a decay time of  $T_3 = 0.3 \text{ ps}$ . Therefore, only  $\text{Im}(\epsilon_3) \neq 0$ . The vibronic couplings and the solvent interactions associated with each monomer are modeled by an Ohmic spectral density

$$J(\omega) = 2\pi\hbar\xi\omega\exp(-\omega/\omega_{\text{cutoff}}) \quad (7)$$

where  $\xi = 0.121$  and  $\omega_{\text{cutoff}} = 900 \text{ cm}^{-1}$  corresponding to a reorganization energy  $\lambda_0 = 217.8 \text{ cm}^{-1}$ . The temperature is set to 300 K. (This particular system will be used in different contexts throughout the paper. For simplicity, we will refer to it as the “excitonic trimer.”) The transport starts with excitation on the first monomer,  $\tilde{\rho}(0) = |1\rangle\langle 1|$ . The loss  $L(t)$  for the excitonic trimer is shown in Figure 1. The emergent time-scale of loss, obtained with the model fit  $L(t) = 1 - \exp(-t/\tau)$ , is  $\tau = 1.04 \text{ ps}$ , which is significantly longer than the local loss time-scale of  $T_3 = 0.3 \text{ ps}$ .

If we were interested in the transport through a system with only one trap site, then considering the dynamics of  $L(t)$  as demonstrated would be adequate. However, we want to generalize this to molecular aggregates with multiple traps, where we would like to extract the trap-specific efficiency. The primary complication that arises with the previous argument of the loss being the deviation of the trace of the density matrix from unity applied to this case is that the loss can now occur through more than one site. How do we determine the partitioning of this total loss into the constituent single-site

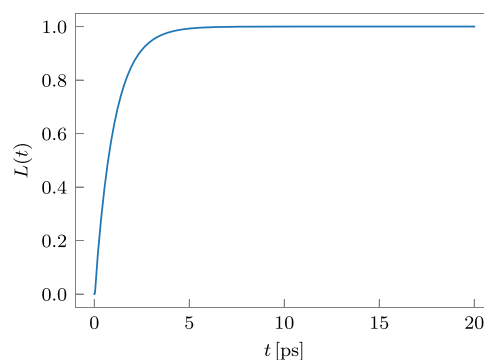


**Figure 1.** Excitation loss  $L(t) = 1 - \text{Tr}[\tilde{\rho}(t)]$  in the excitonic trimer with a single trap starting with an initial excitation  $\tilde{\rho}(0) = |1\rangle\langle 1|$  and  $T_3 = 0.3 \text{ ps}$ .

losses? To achieve this, we generalize the concept of state-to-state transfer<sup>31</sup> and the related idea of coherence maps<sup>40–42</sup> to account for non-Hermitian systems.

The state-to-state framework<sup>31</sup> begins by considering the rate of change of population of the  $j$ th site

$$\frac{\partial P_j(t)}{\partial t} = \frac{\partial}{\partial t} \text{Tr}_{\text{sys-env}}[\rho(t)|j\rangle\langle j|] \quad (8)$$

where  $\rho(t)$  is the time-evolved density matrix in the full system–environment Hilbert space. Because the Hamiltonian is non-Hermitian, the quantum Liouville equation gets reformulated as

$$\frac{\partial \rho(t)}{\partial t} = -\frac{i}{\hbar}(\hat{H}\rho(t) - \rho(t)\hat{H}^\dagger) \quad (9)$$

Consequently, eq 8 can be written as

$$\frac{\partial P_j(t)}{\partial t} = -\frac{i}{\hbar} \text{Tr}_{\text{sys-env}}[(\hat{H}\rho(t) - \rho(t)\hat{H}^\dagger)|j\rangle\langle j|] \quad (10)$$

$$= \frac{i}{\hbar} \text{Tr}_{\text{sys}}[\tilde{\rho}(t)(\hat{H}_0^\dagger|j\rangle\langle j| - |j\rangle\langle j|\hat{H}_0)] \quad (11)$$

using the fact that the projector,  $|j\rangle\langle j|$ , commutes with  $\hat{H}_{\text{env}}$ . Expanding the trace, we can partition this flux into the following source sites:

$$\frac{\partial P_j(t)}{\partial t} = \frac{i}{\hbar} \sum_k (\langle j|\tilde{\rho}(t)|k\rangle\langle k|\hat{H}_0^\dagger|j\rangle - \langle j|\hat{H}_0|k\rangle\langle k|\tilde{\rho}(t)|j\rangle) \quad (12)$$

For every  $k$ , the summand expresses the instantaneous rate of transfer from  $k$  to  $j$ , and the total rate of change of the population of the  $j$ th site is given as a sum over all  $k$ , as expressed in eq 12. Integrating over time, one gets the total partitioned transfer between the  $k$ th and the  $j$ th sites until time  $t$ ,

$$\begin{aligned} P_{j\leftarrow k}(t) &= \frac{i}{\hbar} \int_0^t dt' (\langle k|\hat{H}_0^\dagger|j\rangle - \langle j|\hat{H}_0|k\rangle) \text{Re}\langle j|\tilde{\rho}(t')|k\rangle \\ &\quad - \frac{1}{\hbar} \int_0^t dt' (\langle k|\hat{H}_0^\dagger|j\rangle + \langle j|\hat{H}_0|k\rangle) \text{Im}\langle j|\tilde{\rho}(t')|k\rangle \end{aligned} \quad (13)$$

For Hermitian systems, only the second term survives, and the expression reduces to the previously derived expression for state-to-state transport.<sup>31,32</sup> The state-to-state analysis as done

previously is closely related to the coherence maps developed by Makri and co-workers.<sup>40–42</sup> Similar terms also appear in analyses involving flux networks, which have been used for understanding and quantifying robustness of transport by Wu et al.<sup>43</sup> The extra physics corresponding to the non-Hermitian losses are all incorporated in the first term. Because non-Hermiticity is limited to the diagonal on-site terms, note that the site-to-site transport ( $j \neq k$ ) is still governed only by the second term, which becomes  $P_{j \leftarrow k}(t) = -\frac{2}{\hbar} \int_0^t dt' \langle j | \hat{H}_0 | k \rangle \text{Im} \langle j | \tilde{\rho}(t') | k \rangle$ . For the self-transfer terms ( $j = k$ ), the second term becomes zero because the diagonal elements of the density matrix are real. However, the first term is nonzero with  $P_{j \leftarrow j}(t) = \frac{2}{\hbar} \int_0^t dt' \text{Im} \langle j | \hat{H}_0 | j \rangle \text{Re} \langle j | \tilde{\rho}(t') | j \rangle$ . Notice that if a site has a loss term,  $\text{Im} \langle j | \hat{H}_0 | j \rangle < 0$  and  $P_{j \leftarrow j}(t) < 0$ , symbolizing a loss from the site into the environment. Thus, the loss through the  $j$ th site,  $L_j(t)$ , is identified with  $P_{j \leftarrow j}(t)$ , and the total loss can be expressed as a sum over all of the site-based losses. To obtain the emergent time-scale, this can now be fit to the following model (assuming a single exponential decay):

$$L_j(t) = L_j^\infty (1 - \exp(-t/\tau_j)) \quad (14)$$

where  $\tau_j$  is the emergent decay time for site  $j$  and  $L_j^\infty$  is the net loss through that site. These quantities will now be used to characterize the efficiency of transport with a single time-scale. Notice that  $L_j(0) = 0$  and  $\lim_{t \rightarrow \infty} L_j(t) = L_j^\infty$ .

A few additional words are due to eq 13. While this paper is about transport efficiencies specific to drain sites, which are exemplified by Hamiltonians with diagonal non-Hermiticities, other kinds of non-Hermiticities are also ubiquitous in the literature. One very common model is the Hatano–Nelson model,<sup>44,45</sup> which is a non-Hermitian tight-binding model where the non-Hermiticity is caused by  $\langle j | \hat{H}_0 | k \rangle \neq \langle k | \hat{H}_0 | j \rangle^*$  for  $j \neq k$ .<sup>46</sup> These are interesting because they show the so-called non-Hermitian skin effect. If the system were described by such a model, the state-to-state analysis described by eq 13 would still be valid.

### 3. NUMERICAL RESULTS

In order to demonstrate this non-Hermitian state-to-state method, we consider a polaritonic system—the same excitonic trimer of identical monomers as discussed earlier—now coupled to a leaky Fabry–Pérot cavity of energy  $\hbar\omega_c$  with a coupling strength of  $\Omega = 181.5 \text{ cm}^{-1}$ . The cavity mode energy is set in resonance with the monomer's vertical or FC excitation energy, that is,  $\hbar\omega_c = \epsilon = 0 \text{ cm}^{-1}$ . (The method developed here is independent of the system. As an illustration, another interesting setup is provided in Appendix A, where the cavity is taken to be resonant with the molecular 0–0 transition.) The new system Hamiltonian  $\hat{H}_0'$  is given by

$$\hat{H}_0' = \hat{H}_0 + \hbar(\omega_c - i\pi/T_c) |c\rangle \langle c| + \sum_j \Omega |j\rangle \langle c| + |c\rangle \langle j| \quad (15)$$

where  $|c\rangle$  is the cavity mode. The cavity mode has a lifetime  $T_c$  of 0.6 ps, corresponding to a decay rate of 6.9 meV, which is smaller than the typical decay rate of 50 meV for plasmonic or dielectric cavities.<sup>47</sup> For  $\hbar\omega_c$  corresponding to 800 nm (typical excitation energy of bacteriochlorophyll chains),<sup>37–39</sup> the quality factor ( $Q = \omega_c T_c$ ) of the cavity comes out to be

1413. Also, note that the cavity is not associated with any bath. (This system will be called the “polaritonic trimer.”)

The initial excitation is again set to be on the first monomer,  $\tilde{\rho}(0) = |1\rangle \langle 1|$ . The loss from the third monomer (exciton drain) and the cavity is shown in Figure 2. As mentioned, the

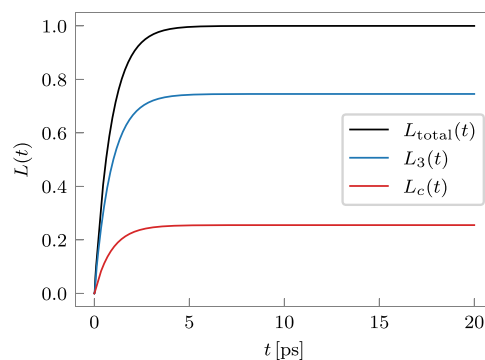


**Figure 2.** Total (black) and trap-dependent (blue and red) excitation losses in the polaritonic trimer starting with an initial excitation  $\tilde{\rho}(0) = |1\rangle \langle 1|$  through an exciton drain of decay time  $T_3 = 0.3 \text{ ps}$  coupled to a leaky optical cavity of lifetime  $T_c = 0.6 \text{ ps}$ .

total loss,  $L(t)$ , is the sum of losses from the exciton drain,  $L_3(t)$ , and the cavity,  $L_c(t)$ . The emergent loss time-scales for the exciton drain,  $\tau_3$ , and cavity,  $\tau_c$ , are 0.89 and 0.90 ps, respectively. In this case, a large majority (around 74%) of the extraction happens through the molecular drain site.

It is pertinent at this point to ask how exactly the excitation flows through the system to reach these leaky sites. A state-to-state analysis is presented in Figure 3 to show the excitation flows to the leaky sites along with their populations. Notice that at very short times, the flow from the nonleaky sites,  $|1\rangle$  and  $|2\rangle$ , into the cavity  $|c\rangle$  (Figure 3b) is more than that into the exciton drain site  $|3\rangle$  (Figure 3a). This is because both  $|1\rangle$  and  $|2\rangle$  transfer population to the cavity site, whereas only  $|2\rangle$

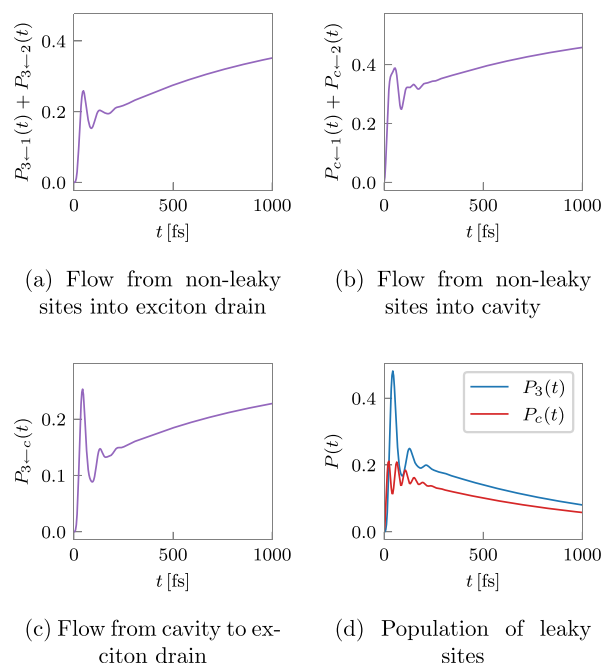


**Figure 3.** State-to-state analysis of excitation flows into trap sites and their population dynamics for the polaritonic trimer.

transfers to  $|3\rangle$  owing to the nearest-neighbor nature of the excitonic Hamiltonian. However, very soon, the transfer from  $|2\rangle$  to  $|3\rangle$  catches up. What is very interesting is that there is a significant flow from the cavity site  $|c\rangle$  to the exciton drain site  $|3\rangle$  from very early times (Figure 3c). All of this, along with the leakages from  $|c\rangle$  and  $|3\rangle$ , comes together to give the total population dynamics that we can see in Figure 3d. Notice that the initial buildup of population is higher in  $|3\rangle$  than in the cavity, even though the leakage on the cavity in this case is slower than that of the monomer.

Now, let us see what happens when the reorganization energy of the monomeric environment increases. The losses through the exciton drain  $L_3(t)$  for the same system Hamiltonian parameters but with different bath reorganization energies are presented in Figure 4. (Note that the time-axis is

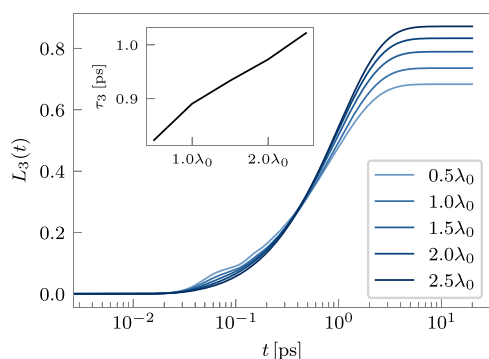


**Figure 4.** Loss through exciton drain  $L_3(t)$  with increasing bath reorganization energies,  $\lambda$ , and the emergent time-scales  $\tau_3$  (inset) for the polaritonic trimer.

on the log-scale.) We change the Kondo parameter  $\xi$  (eq 7) to change the bath reorganization energy  $\lambda$ . It is clear that the amount of extraction through the third monomer ( $L_3^\infty$ ) increases with reorganization energy. As a corollary, this would imply that the amount of leakage through the cavity is decreasing. To understand this better, recall that the cavity energy is set to be resonant with the FC (vertical) excitation energy of the monomer. The higher the reorganization energy, the greater is the shift between the ground and excited states of each of the monomers because the reorganization energy per “mode” is proportional to the Huang–Rhys factor and consequently the relative displacement of the surfaces. In Figure 5, a schematic is shown of the current situation. Suppose that  $|e\rangle$  is the excited-state surface for the lower reorganization energy environment and  $|e'\rangle$  is the one for the higher reorganization energy environment of a monomer. Notice that  $d' > d$ . Now, to ensure that the vertical excitation energy remains constant, the surface of  $|e'\rangle$  has to be stabilized more. This means that the minimum of the excited-state potential energy surface becomes increasingly detuned from the cavity energy, hampering the transport into the cavity mode from the monomers.

There is a completely different parallel picture for understanding the changes in  $L_3^\infty$  with the reorganization energy. While we were considering the monomers to be the “units” up to now, our system is, in fact, an excitonic aggregate in a cavity. For such aggregates, these monomeric states are diabatic, and the cavity can equivalently be thought of as coupling to the aggregate adiabatic eigenstates. Therefore, in addition to the shifting of the monomeric potential energy landscape with

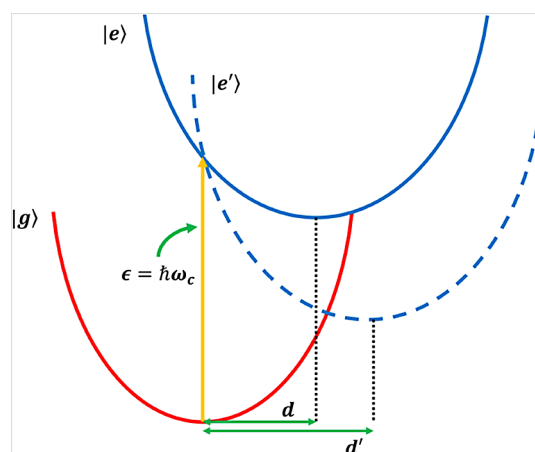


**Figure 5.** Schematic depicting a shift in excited energy surfaces for two baths differing in their reorganization energies. The  $|e\rangle$  surface corresponds to the higher reorganization energy bath than the  $|e'\rangle$  surface leading to a larger displacement  $d' > d$ .

reorganization energy, an added complication is deciding where the bright states of the aggregate lie. For an *H*-like aggregate, the bright state has a higher energy than the monomeric energies, whereas for a *J*-like aggregate, it is lower. Consequently, the level of detuning that the cavity mode suffers from, from the bright adiabat, is also dependent on the nature of the aggregate. In our case, the excitonic aggregate is *J*-like, which exaggerates the detuning that is already caused by the increasing reorganization energy. As a demonstration of this argument, we provide two pieces of evidence. First, we have simulated the spectrum of the lossy excitonic trimer using our PILD method,<sup>28,29</sup> which is shown in Figure 6. Remember

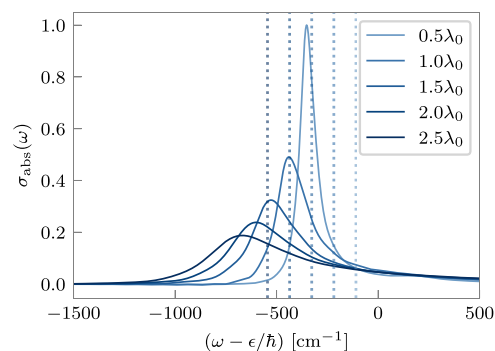


**Figure 6.** Absorption spectra for the linear excitonic trimer for different reorganization energies,  $\lambda$ , normalized with respect to the maximum intensity for the spectrum corresponding to  $\lambda = 0.5\lambda_0$ . The vertical dotted lines mark the energy corresponding to  $\epsilon - \lambda$ , that is, the energy of the molecular 0–0 transition.

that the cavity has energy  $\hbar\omega_c = \epsilon$ , which is at the origin of the  $x$ -axis in the plot. On increasing the reorganization energy, the maximum of the peak gets red-shifted significantly, thereby increasingly detuning the cavity from the bright state. Next, in Figure 7, we show the population of the cavity site. Notice that the accumulation of excitation in the cavity mode decreases with an increasing reorganization energy on the monomers, which is a result of this detuning.

Having discussed the increase in  $L_3^\infty$  as a function of  $\lambda$ , we turn our attention to the emergent time-scales. While the initial slopes of the loss curves in Figure 4 are not the same, they are

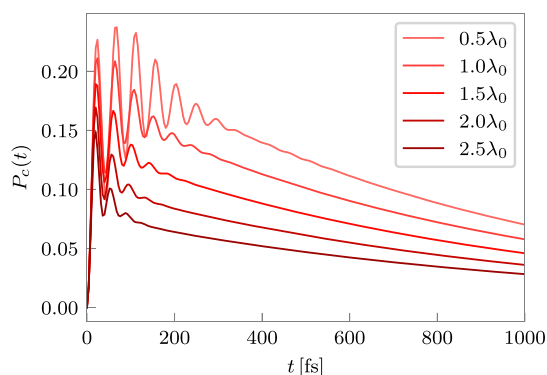


**Figure 7.** Population of the cavity site,  $P_c(t)$ , for different reorganization energies,  $\lambda$ , in the polaritonic trimer.

similar. After the initial transients that make the losses higher for smaller reorganization energies on a time-scale of hundreds of femtoseconds, the slopes increase with the reorganization energy. This leads to a crossover of the loss curves around 400 fs. However, this “small” difference of gradients at short times is not substantial enough to overcome the difference in the long time loss amounts,  $L_3^\infty$ . Thus, the emergent time-scales,  $\tau_3$ , in these cases, are dominated primarily by the  $L_3^\infty$  and increase with the reorganization energy,  $\lambda$ .

It should be noted here that it is not necessary that the loss dynamics have a single time-scale. In fact, the exponential fit to the loss function, eq 14, begins to fail when the reorganization energy of the environment decreases beyond a certain limit due to a preponderance of transients in the dynamics. This parallels the failure of the rate theory to predict the actual dynamics when transients are important.<sup>48</sup> For a particular example, notice the “bumps” in the low reorganization energy loss curves in Figure 4 at around 100 fs. Those are deviations from single time-scale dynamics. However, in this particular example, these deviations are small enough that the overall loss dynamics is still well-approximated by a single time-scale dynamics. There could be other examples where the deviations are even more significant. The present non-Hermitian state-to-state analysis method can be used even when this happens. It is just that we would not be able to talk in terms of the emergent time-scales and would have to directly study the loss curves similar to the ones in Figure 4.

As a final bit of exploration, let us see how the transport efficiency of the exciton drain gets affected vis-à-vis the change in cavity properties—monomer–cavity coupling,  $\Omega$ , and cavity leakage rate,  $\gamma_c$  ( $= 1/T_c$ ). It is more meaningful to vary these parameters relative to their monomeric counterparts— $h$  and  $\gamma_3$  ( $= 1/T_3$ ). Figure 8a,b shows the change of  $L_3^\infty$  and  $\tau_3$ , respectively, as functions of  $\gamma_c/\gamma_3$  for different cavity couplings  $\Omega/h$  keeping the environment at a constant reorganization energy of  $\lambda_0$ . First, consider the amount of excitation extracted from the third monomer,  $L_3^\infty$ , shown in Figure 8a. As a function of  $\gamma_c/\gamma_3$ , it goes down monotonically because for the same  $\Omega/h$ , when  $\gamma_c$  increases relative to  $\gamma_3$ , then more loss happens out of the cavity. What is interesting is that for a particular  $\gamma_c/\gamma_3$ , the value of  $L_3^\infty$  decreases on increasing  $\Omega/h$ . To understand this better, we plot the excitonic population of the third monomer and the cavity as a function of time for the three values of  $\Omega/h$  at a constant  $\gamma_c/\gamma_3 = 0.25$  in Figure 8c,d, respectively. Notice that as  $\Omega/h$  increases, the amount of population buildup on the cavity increases, but the accumulation on the third monomer decreases. One can

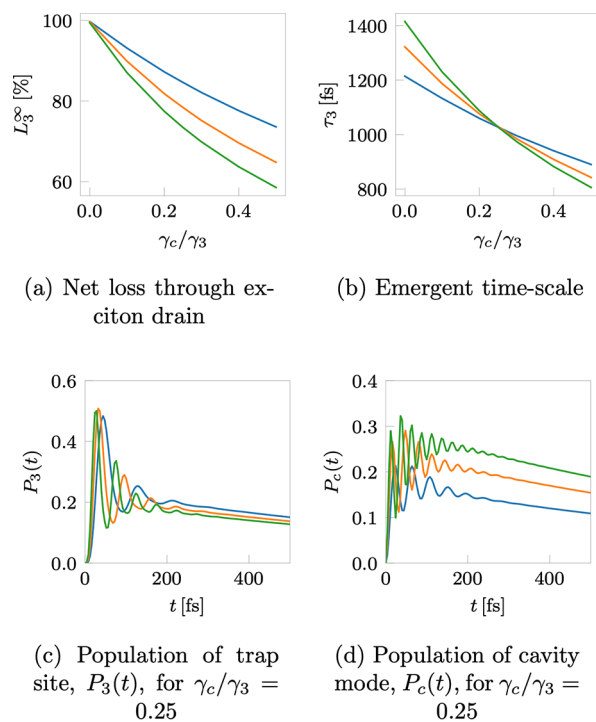


**Figure 8.** Analysis of loss mechanisms in the polaritonic trimer. Line color denotes the relative coupling strength: blue line,  $\Omega/h = 1.0$ ; orange line,  $\Omega/h = 1.5$ ; green line,  $\Omega/h = 2.0$ . Subfigures (a) and (b) study the system as a function of changing relative loss rates. Subfigures (c) and (d) analyze the populations of the third monomer and the cavity for different  $\Omega/h$  values at a constant  $\gamma_c/\gamma_3$ .

intuitively understand this by considering the couplings in the aggregate and the relative flows. There are three connections into the cavity state each with a coupling of  $\Omega$ , and there are two connections into the third monomer, one with  $\Omega$  and one with  $h$ . At time  $t = 0$ , the excitation is localized on monomer 1. As it starts to flow, the excitation finds one route with a coupling of  $h$  and another route with a coupling of  $\Omega > h$ . Consequently, more excitation flows into the cavity via the channel with a strength  $\Omega$ . Thereafter, depending on the relative magnitudes of  $\Omega$  and  $h$ , from every monomer, there is a greater amount of excitation that leaks into the cavity than into the next monomer, leading to the observation. This correspondingly means that there is comparatively less population to be extracted out of  $|3\rangle$ , leading to a decrease in  $L_3^\infty$ .

In Figure 8b, we see that the  $\tau_3$  values for a constant  $\Omega/h$  decrease monotonically with  $\gamma_c/\gamma_3$  as well. Probably, this is related to having a lower amount of exciton extracted from the molecular drain ( $L_3^\infty$ ). We conclude our discussion of this particular problem by pointing out a surprising observation for future exploration: the  $\tau_3$  curves for different  $\Omega/h$  values in Figure 8b all intersect at a point for  $\gamma_c/\gamma_3 = 0.25$ . This raises several very interesting questions: Why do we have this point of intersection? Do polaritonic aggregates of different sizes all have similar points of intersection? How does it change with changing the bath on each site? These interesting problems will be dealt with in a future publication using the non-Hermitian state-to-state analysis technique developed in the current work.

#### 4. CONCLUSIONS

In this paper, we have developed a generalization of the state-to-state analysis<sup>31,49</sup> to account for non-Hermitian systems coupled with thermal environments. This development additionally enables us to analyze the endpoint or trap-specific efficiency of a multitrapped transport aggregate, where the extraction is encoded through diagonal imaginary terms in the system Hamiltonian. This method is exact when paired with exact dynamics and makes no additional approximations. While here we have explored the time-scales of transport, there can be several cases where the extraction process may not be appropriately described by a curve with a single time-scale. For such cases, the current non-Hermitian state-to-state analysis technique can yield the full dynamics of the extraction. In addition, being a generalization of the state-to-state analysis technique,<sup>31</sup> this method also allows us to explore the exact pathways of transport under these leakages. In the examples shown, we demonstrated how the non-Hermitian state-to-state method can be used to understand transport in a polaritonic aggregate, where the exciton is extracted from one of the molecules, and the cavity is lossy. Of course, in such a case, any loss of the excitation as a photon through the cavity does not count toward transport. Using our non-Hermitian state-to-state method, we are able to partition the total loss into the loss through the cavity and through the molecule. In the process, we reveal a wealth of rich physics. While the examples shown here used exact dynamics generated using path integrals, one could as well use approximate semiclassical or perturbative methods to generate the dynamics. This method promises to be a powerful analysis tool for understanding the dynamics of complex systems.

#### ■ TRANSPORT EFFICIENCY FOR THE CAVITY RESONANT WITH MOLECULAR 0–0 TRANSITION

The analysis for the polaritonic trimer presented so far has the cavity resonant with the molecular or monomeric FC excitation ( $\hbar\omega_c = \epsilon = 0 \text{ cm}^{-1}$ ). A similar analysis can be done when the cavity is made resonant with the molecular 0–0 transition ( $\hbar\omega_c = \epsilon - \lambda = -217.8 \text{ cm}^{-1}$ , where  $\lambda$  is the reorganization energy corresponding to the molecular environment). For convenience, we will now refer to these cases as FC and 0–0, respectively. It is to be noted that the state-to-state method is independent of the excitation to which the cavity is set in resonance with.

In Figure 9, the losses through the exciton drain, cavity, and the total loss in the polaritonic trimer are presented for the cavity in resonance with the molecular 0–0 transition along with that of the FC case as depicted in Figure 2. The emergent loss time-scales in the 0–0 case for the exciton drain,  $\tau_3$ , and cavity,  $\tau_c$ , are 0.82 and 0.86 ps, respectively. In this case, like the FC case, the majority of the loss (around 60%) occurs through the exciton drain, which, however, is less than the corresponding 74% in the FC case. The loss through the cavity increases in the 0–0 case compared to the FC case. This happens because the cavity is comparatively less detuned from the vibronic absorption maximum of the excitonic trimer in the 0–0 case, making excitation flow into the cavity more facile as compared to the FC case.

Next, consider the analysis of the loss curves as a function of the reorganization energy that we did for the FC case. In that case, we have discussed why the level of detuning of the cavity vis-à-vis the absorption maximum is highly dependent on the

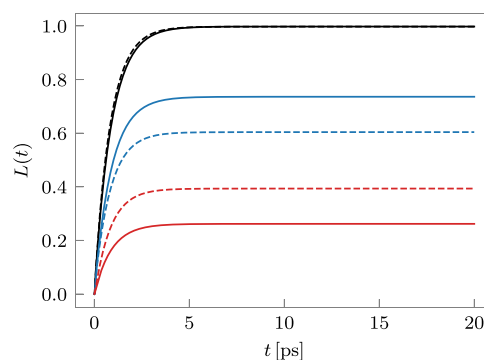


**Figure 9.** Excitation loss through the exciton drain  $L_3(t)$  (blue) and the cavity  $L_c(t)$  (red) in the polaritonic trimer starting with an initial excitation  $\tilde{\rho}(0) = |1\rangle\langle 1|$  for an exciton drain of decay time  $T_3 = 0.3 \text{ ps}$  and a leaky optical cavity of lifetime  $T_c = 0.6 \text{ ps}$  resonant with the FC (solid) and molecular 0–0 (dashed) excitations. The total loss  $L_{\text{total}}(t)$  is depicted in black.

reorganization energy. What happens now that we are considering the cavity to be resonant to the molecular 0–0 transition? The energy of the molecular 0–0 transition, as mentioned before, is  $\epsilon - \lambda$ , which already “accounts for” the reorganization energy. In the context of the schematic in Figure 5, the molecular 0–0 transition is the energy gap between the bottom of the red surface and the bottom of the blue surface. The molecular absorption maximum will be at an energy higher than the 0–0 transition but significantly lower than the FC transition energy. Therefore, the level of detuning that we will see as we change the reorganization energy is going to be smaller. In Figure 10, we show a comparison of the

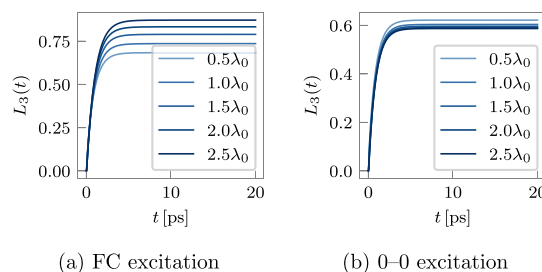


**Figure 10.** Dependence of  $L_3^\infty$  for the FC resonant and the molecular 0–0 resonant cavities. Data for subfigure (a) are identical to those in Figure 4.

loss curves through the exciton drain,  $L_3(t)$ , for the different cases. As expected, the band of  $L_3^\infty$  for the case when the cavity is FC resonant is much broader than that of the 0–0 resonance case.

In the body of the paper, we have already justified the order of the curves for the FC resonant case, Figure 10a or Figure 4. The value of  $L_3^\infty$  increases with the reorganization energy in this case. However, notice that the order is reversed for the 0–0 resonant case in Figure 10b. To understand this better, we revisit Figure 6. Focus on the vertical dotted lines now, which are at  $\epsilon - \lambda$  or the energy of the molecular 0–0 transition. For all of the different reorganization energies considered, this is much closer to the energy of the absorption maximum than the FC excitation energy, in accordance with our argument. This ensures that the band spanned by  $L_3^\infty$  in the case of the 0–0 resonant cavity is smaller than for the FC resonant cavity. To understand the changed order of  $L_3^\infty$  with respect to  $\lambda$  in Figure

10b, two other factors need to be discussed. The distance between the molecular 0–0 transition energy and the absorption maximum in Figure 6 decreases monotonically with the increasing reorganization energy from  $243\text{ cm}^{-1}$  for  $\lambda = 0.5\lambda_0$  to  $124\text{ cm}^{-1}$  for  $\lambda = 2.5\lambda_0$ . Additionally, the peak broadening also increases with increasing  $\lambda$ . This further decreases the effective detuning of the cavity. As a result of the combination of the two effects, the cavity becomes more in resonance with the bright state as the reorganization energy increases and is able to funnel off increasing amounts of exciton. Thus,  $L_3^\infty$  decreases with increasing  $\lambda$ , and we see the pattern in Figure 10b.

## AUTHOR INFORMATION

### Corresponding Author

Amartya Bose – Department of Chemical Sciences, Tata Institute of Fundamental Research, Mumbai 400005, India;  
orcid.org/0000-0003-0685-5096; Email: amartya.bose@tifr.res.in, amartya.bose@gmail.com

### Author

Devansh Sharma – Department of Chemical Sciences, Tata Institute of Fundamental Research, Mumbai 400005, India

Complete contact information is available at:  
<https://pubs.acs.org/10.1021/acs.jctc.5c00497>

### Notes

The authors declare no competing financial interest.

## REFERENCES

- Engel, G. S.; Calhoun, T. R.; Read, E. L.; Ahn, T.-K.; Mančal, T.; Cheng, Y.-C.; Blankenship, R. E.; Fleming, G. R. Evidence for Wavelike Energy Transfer through Quantum Coherence in Photosynthetic Systems. *Nature* **2007**, *446*, 782–786.
- Ishizaki, A.; Fleming, G. R. Theoretical Examination of Quantum Coherence in a Photosynthetic System at Physiological Temperature. *Proc. Natl. Acad. Sci. U. S. A.* **2009**, *106*, 17255–17260.
- Duan, H.-G.; Prokhorenko, V. I.; Cogdell, R. J.; Ashraf, K.; Stevens, A. L.; Thorwart, M.; Miller, R. J. D. Nature Does Not Rely on Long-Lived Electronic Quantum Coherence for Photosynthetic Energy Transfer. *Proc. Natl. Acad. Sci. U. S. A.* **2017**, *114*, 8493.
- Duan, H.-G.; Jha, A.; Chen, L.; Tiwari, V.; Cogdell, R. J.; Ashraf, K.; Prokhorenko, V. I.; Thorwart, M.; Miller, R. J. D. Quantum Coherent Energy Transport in the Fenna–Matthews–Olson Complex at Low Temperature. *Proc. Natl. Acad. Sci. U. S. A.* **2022**, *119*, No. e2212630119.
- White, S. R. Density Matrix Formulation for Quantum Renormalization Groups. *Phys. Rev. Lett.* **1992**, *69*, 2863–2866.
- Schollwöck, U. The Density-Matrix Renormalization Group. *Rev. Mod. Phys.* **2005**, *77*, 259–315.
- Schollwöck, U. The Density-Matrix Renormalization Group in the Age of Matrix Product States. *Annals of Physics* **2011**, *326*, 96–192.
- Meyer, H.-D.; Manthe, U.; Cederbaum, L. The Multi-Configurational Time-Dependent Hartree Approach. *Chem. Phys. Lett.* **1990**, *165*, 73–78.
- Beck, M.; Jäckle, A.; Worth, G. A.; Meyer, H.-D. The Multiconfiguration Time-Dependent Hartree (MCTDH) Method: A Highly Efficient Algorithm for Propagating Wavepackets. *Phys. Rep.* **2000**, *324*, 1–105.
- Heijs, D.-J.; Malyshev, V. A.; Knoester, J. Trapping Time Statistics and Efficiency of Transport of Optical Excitations in Dendrimers. *J. Chem. Phys.* **2004**, *121*, 4884–4892.
- Cao, J.; Silbey, R. J. Optimization of Exciton Trapping in Energy Transfer Processes. *J. Phys. Chem. A* **2009**, *113*, 13825–13838.
- Sener, M. K.; Lu, D.; Ritz, T.; Park, S.; Fromme, P.; Schulten, K. Robustness and Optimality of Light Harvesting in Cyanobacterial Photosystem I. *J. Phys. Chem. B* **2002**, *106*, 7948–7960.
- Uchiyama, C.; Munro, W. J.; Nemoto, K. Environmental Engineering for Quantum Energy Transport. *npj Quantum Inf.* **2018**, *4*, 33.
- Dijkstra, A. G.; Beige, A. Efficient Long-Distance Energy Transport in Molecular Systems through Adiabatic Passage. *J. Chem. Phys.* **2019**, *151*, No. 034114.
- Kreisbeck, C.; Kramer, T.; Rodríguez, M.; Hein, B. High-Performance Solution of Hierarchical Equations of Motion for Studying Energy Transfer in Light-Harvesting Complexes. *J. Chem. Theory Comput.* **2011**, *7*, 2166–2174.
- Tanimura, Y.; Kubo, R. Time Evolution of a Quantum System in Contact with a Nearly Gaussian-Markoffian Noise Bath. *J. Phys. Soc. Jpn.* **1989**, *58*, 101–114.
- Tanimura, Y. Reduced Hierarchical Equations of Motion in Real and Imaginary Time: Correlated Initial States and Thermodynamic Quantities. *J. Chem. Phys.* **2014**, *141*, No. 044114.
- Tanimura, Y. Numerically “Exact” Approach to Open Quantum Dynamics: The Hierarchical Equations of Motion (HEOM). *J. Chem. Phys.* **2020**, *153*, No. 020901.
- Xu, M.; Yan, Y.; Shi, Q.; Ankerhold, J.; Stockburger, J. T. Taming Quantum Noise for Efficient Low Temperature Simulations of Open Quantum Systems. *Phys. Rev. Lett.* **2022**, *129*, No. 230601.
- Ikeda, T.; Scholes, G. D. Generalization of the Hierarchical Equations of Motion Theory for Efficient Calculations with Arbitrary Correlation Functions. *J. Chem. Phys.* **2020**, *152*, 204101.
- Makri, N.; Makarov, D. E. Tensor Propagator for Iterative Quantum Time Evolution of Reduced Density Matrices. I. Theory. *J. Chem. Phys.* **1995**, *102*, 4600–4610.
- Makri, N.; Makarov, D. E. Tensor Propagator for Iterative Quantum Time Evolution of Reduced Density Matrices. II. Numerical Methodology. *J. Chem. Phys.* **1995**, *102*, 4611–4618.
- Makri, N.; Sim, E.; Makarov, D. E.; Topaler, M. Long-Time Quantum Simulation of the Primary Charge Separation in Bacterial Photosynthesis. *Proc. Natl. Acad. Sci. U. S. A.* **1996**, *93*, 3926–3931.
- Strathearn, A.; Kirton, P.; Kilda, D.; Keeling, J.; Lovett, B. W. Efficient Non-Markovian Quantum Dynamics Using Time-Evolving Matrix Product Operators. *Nat. Commun.* **2018**, *9*, 3322.
- Bose, A. Pairwise Connected Tensor Network Representation of Path Integrals. *Phys. Rev. B* **2022**, *105*, No. 024309.
- Bose, A.; Walters, P. L. A Multisite Decomposition of the Tensor Network Path Integrals. *J. Chem. Phys.* **2022**, *156*, No. 024101.
- Bose, A. Quantum Correlation Functions through Tensor Network Path Integral. *J. Chem. Phys.* **2023**, *159*, 214110.
- Bose, A. Incorporation of Empirical Gain and Loss Mechanisms in Open Quantum Systems through Path Integral Lindblad Dynamics. *J. Phys. Chem. Lett.* **2024**, *15*, 3363–3368.
- Sharma, D.; Bose, A. Impact of Loss Mechanisms on Linear Spectra of Excitonic and Polaritonic Aggregates. *J. Chem. Theory Comput.* **2024**, *20*, 9522–9532.
- Palm, T.; Nalbach, P. Nonperturbative Environmental Influence on Dephasing. *Phys. Rev. A* **2017**, *96*, No. 032105.
- Bose, A.; Walters, P. L. Impact of Solvent on State-to-State Population Transport in Multistate Systems Using Coherences. *J. Chem. Theory Comput.* **2023**, *19*, 4828–4836.
- Bose, A.; Walters, P. L. Impact of Spatial Inhomogeneity on Excitation Energy Transport in the Fenna–Matthews–Olson Complex. *J. Phys. Chem. B* **2023**, *127*, 7663–7673.
- Makri, N. The Linear Response Approximation and Its Lowest Order Corrections: An Influence Functional Approach. *J. Phys. Chem. B* **1999**, *103*, 2823–2829.
- Bose, A. Zero-Cost Corrections to Influence Functional Coefficients from Bath Response Functions. *J. Chem. Phys.* **2022**, *157*, No. 054107.
- Feynman, R. P.; Vernon, F. L. The Theory of a General Quantum System Interacting with a Linear Dissipative System. *Annals of Physics* **1963**, *24*, 118–173.

- (36) Bose, A. QuantumDynamics.Jl: A Modular Approach to Simulations of Dynamics of Open Quantum Systems. *J. Chem. Phys.* **2023**, *158*, 204113.
- (37) Tretiak, S.; Middleton, C.; Chernyak, V.; Mukamel, S. Bacteriochlorophyll and Carotenoid Excitonic Couplings in the LH2 System of Purple Bacteria. *J. Phys. Chem. B* **2000**, *104*, 9540–9553.
- (38) Freiberg, A.; Rätsep, M.; Timpmann, K.; Trinkunas, G. Excitonic Polarons in Quasi-One-Dimensional LH1 and LH2 Bacteriochlorophyll a Antenna Aggregates from Photosynthetic Bacteria: A Wavelength-Dependent Selective Spectroscopy Study. *Chem. Phys.* **2009**, *357*, 102–112.
- (39) Bose, A.; Makri, N. All-Mode Quantum–Classical Path Integral Simulation of Bacteriochlorophyll Dimer Exciton-Vibration Dynamics. *J. Phys. Chem. B* **2020**, *124*, 5028–5038.
- (40) Dani, R.; Makri, N. Quantum State-to-State Rates for Multistate Processes from Coherences. *J. Phys. Chem. Lett.* **2022**, *13*, 8141–8149.
- (41) Dani, R.; Makri, N. Time-Evolving Quantum Superpositions in Open Systems and the Rich Content of Coherence Maps. *J. Phys. Chem. B* **2022**, *126*, 9361–9375.
- (42) Dani, R.; Kundu, S.; Makri, N. Coherence Maps and Flow of Excitation Energy in the Bacterial Light Harvesting Complex 2. *J. Phys. Chem. Lett.* **2023**, *14*, 3835–3843.
- (43) Wu, J.; Liu, F.; Ma, J.; Silbey, R. J.; Cao, J. Efficient Energy Transfer in Light-Harvesting Systems: Quantum-classical Comparison, Flux Network, and Robustness Analysis. *J. Chem. Phys.* **2012**, *137*, 174111.
- (44) Hatano, N.; Nelson, D. R. Localization Transitions in Non-Hermitian Quantum Mechanics. *Phys. Rev. Lett.* **1996**, *77*, 570–573.
- (45) Hatano, N.; Nelson, D. R. Non-Hermitian Delocalization and Eigenfunctions. *Phys. Rev. B* **1998**, *58*, 8384–8390.
- (46) Okuma, N.; Sato, M. Non-Hermitian Topological Phenomena: A Review. *Annual Review of Condensed Matter Physics* **2023**, *14*, 83–107.
- (47) del Pino, J.; Schröder, F. A. Y. N.; Chin, A. W.; Feist, J.; Garcia-Vidal, F. J. Tensor Network Simulation of Non-Markovian Dynamics in Organic Polaritons. *Phys. Rev. Lett.* **2018**, *121*, No. 227401.
- (48) Bose, A.; Makri, N. Non-Equilibrium Reactive Flux: A Unified Framework for Slow and Fast Reaction Kinetics. *J. Chem. Phys.* **2017**, *147*, 152723.
- (49) Dani, R.; Makri, N. Excitation Energy Transfer in Bias-Free Dendrimers: Eigenstate Structure, Thermodynamics, and Quantum Evolution. *J. Phys. Chem. C* **2022**, *126*, 10309–10319.